Approachable, Agile, and Precise Spatial Biology with the CellScape Platform

J. Spencer Schwarz,* Daniel Jimenez-Sanchez, Matthew H. Ingalls, Steven T. Lott, Kayla Cashion, Charles Jackson, Arne Christians, Jennifer A. Silverman, Benton Berigan, Thomas D. Campbell, and Oliver Braubach

Bruker Spatial Biology, St. Louis, Missouri

*john.schwarz@bruker.com

Abstract: Understanding the spatial distribution of key cell populations is critical in advancing biomedical research and the development of novel therapeutics. Highly multiplexed biomarker analysis is achieved with single-cell spatial context on the CellScape, a microscopy platform that enables quantitative spatial phenotyping of entire tissue sections mounted on standard histology slides. Leveraging high-resolution, high dynamic range imaging, and automated reagent delivery, the CellScape represents an attractive platform for spatial biology researchers from discovery to translation.

Keywords: spatial biology, multiplex immunofluorescence, photobleaching, HDR microscopy, whole slide imaging

Introduction

Spatial biology is transforming cancer research, immunology, and neuroscience, and it promises to similarly impact other biomedical disciplines. Questions previously thought to be intractable are yielding to comprehensive investigations of intact tissues. Spatial biology spans many modalities, including directed and non-directed transcriptomics, studies of chromatin structure and content, and targeted and non-targeted protein expression mapping [1]. Spatial biology methods are unified by two common characteristics: they generate high-parameter datasets from a single sample— detecting dozens of proteins, hundreds of transcripts, or thousands of genes— and they provide crucial spatial information alongside relevant biological insights.

The development of spatial biology is a reaction to the limitations posed by earlier high-plex analytical methods (flow cytometry, RNA-seq, etc.), which require physical disruption or dissolution of the sample. These methods are incapable of capturing spatial information about cell phenotypes, cell-cell interactions, morphological states, and tissue architecture patterns. Prior to the advent of spatial biology, morphological analyses were limited to low-plex histology methods like immunohistochemistry (IHC) and immunofluorescence (IF), which could only visualize a few biomarkers at a time. Recent breakthroughs that allow analyses of intact tissues alongside high-plex biomarker detection have driven the rapid growth of spatial omics technologies [2].

The non-spatial cognate of IF is flow cytometry, where multiplexing is achieved by simultaneous detection of unique spectral signatures of fluorophore-labeled antibodies. One approach to spatial biology is to port this method to tissue-based IF, but, due to excitation crosstalk and emission bleed-through typical of fluorescent detection, conventional microscopes can only image four or five markers simultaneously. With spectral overlap unmixing, this number can increase to ten to twelve markers [3]. The core challenge for all highly multiplexed IF platforms is developing strategies to overcome spectral crowding.

Cyclic multiplex immunofluorescence (mIF) overcomes the limitations of using the spectral space [4]. The spectral crowding problem is avoided by replacing the single staining step with iterative rounds of low-plex staining and imaging using an epifluorescence microscope. Each imaging round is terminated by the removal of the fluorescent signal. Automating this otherwise-laborious process, the CellScape™ Precise Spatial Multiplexing platform employs reliable and straightforward cyclic mIF imaging for high-plex targeted protein detection and localization *in situ* (Figure 1). This article provides a detailed introduction to data collection and analysis using CellScape for agile, approachable, and precise cyclic mIF-based spatial biology.

Technology – Instrumentation

The CellScape instrument automates cyclic mIF probing of tissue sections as well as fixed cell suspensions. Samples are prepared on standard histology slides and sealed into an imaging chamber that is plumbed to the platform's fluidics unit for automated reagent delivery. Fluorescently labeled molecular probes, typically primary antibodies, are delivered in a mixture of up to five probes per staining round. The sample is then optically scanned. Following image acquisition, samples are exposed to visible light while actively blocking UV or IR wavelengths to photobleach the fluorescent probes. The photobleached probes contribute no further fluorescent signals, and the sample is ready for subsequent rounds of staining (Figure 2). Background fluorescence images are taken before staining and after filtered photobleaching to ensure proper assignment of true biomarker signals, enhancing the accuracy of the analysis by subtracting background fluorescence.

Physically, the instrument is an epifluorescence microscope integrated with an in-process auto-stainer (Figure 3). The microscope is capable of imaging five spectrally discrete fluorescent channels per cyclic staining round, as well as collecting brightfield monochromatic images. It supports automated staining, scanning, and precise probe-filtered photobleaching of up to four independent samples without user intervention. The connected fluidics unit has fifteen reservoirs for delivering mixtures of fluorescent antibody probes to the sample, for a possible total of 75 probes (that is, 5 probes per cycle/per reservoir). Reservoirs may also be exchanged in process, enabling further expansion of the total probe number.

The CellScape scans an entire tissue section and collects and montages an array of images with high spatial resolution, high pixel density, and high-expression fidelity through high dynamic range (HDR) image capture. The optical train delivers

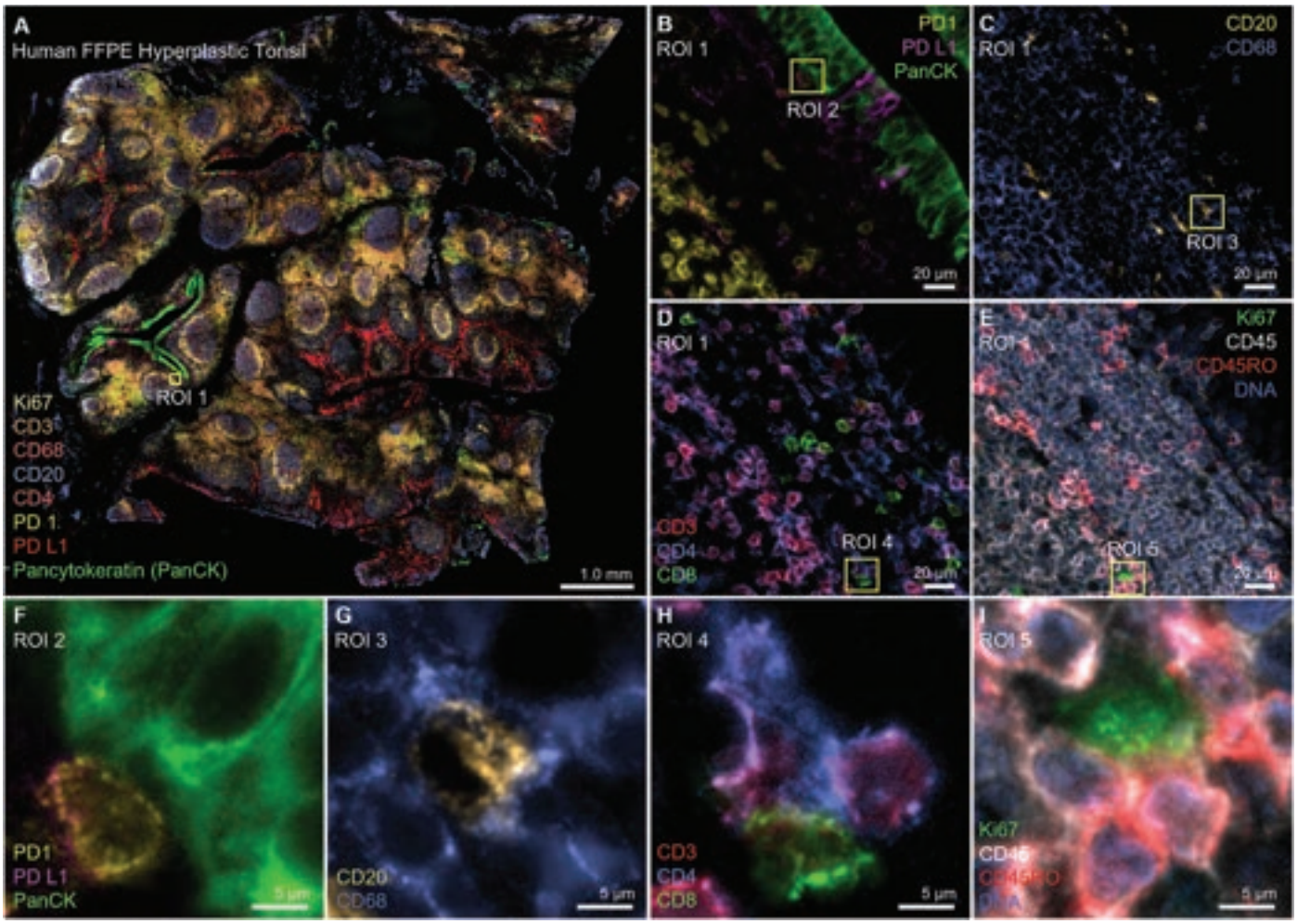

Figure 1: Multiplexed immunofluorescence data acquired from a human hyperplastic tonsil FFPE section using CellScape and the VistaPlex Spatial Immune Profiling Kit. A, Whole-tissue scale of data collection. B–E, Select markers corresponding to ROI 1 from A, denoting a tonsillar crypt margin and highlighting the spatially organized multiplexed information provided by mIF. F–I, ROI 2–5 from B–E, respectively, highlighting sub-cellular biomarker localization provided at scale through high-resolution, high-contrast image capture.

precise image formation through use of a 0.80 NA 20× PlanApo Lambda D objective (Nikon Instruments). Digital sampling of the field-of-view (FOV) at 182 nm per pixel provides Nyquist sampling for any feature larger than ~400 nm. The combination of low-magnification, high numerical aperture, and fine digital sampling provides the brightness and contrast necessary to discern fine details in cells such as chromatin super structure, nuclear envelopes, cell membrane architecture like filopodia, and clear separation of punctate signals that are the basis of biomarker measurements in orthogonal detection strategies (Figure 4). Though this level of detail is not uncommon for fluorescence microscopy, this level of quality is notable within spatial biology, where competing requirements must be balanced, including sample throughput and flow cell architecture.

Cyclic staining presents a device control and data curation challenge: channel registration. Registration requires the reproducible return to a physical sample location, within submicron position, and then alignment of image sequences to single-pixel-level precision. The sophistication of mechanical control and image analysis required to accomplish this feat is not trivial [6]. Fortunately, these capabilities are built into the CellScape system with both precise stage control and image overlay algorithms, removing this concern from the researcher's consideration.

Cycling with Standard Antibodies and Photobleaching

mIF spatial techniques are largely differentiated by their methods for signal removal, and signal removal approaches ultimately define the physical limit of the multiplex [1]. Some example strategies include labeling with oligo barcodes, secondary labeling and stripping, chemically induced fluorescence inactivation, and filtered photobleaching of fluorescence. Each method confers advantages and limitations. Filtered photobleaching of fluorescent probes is arguably the most direct and least damaging method for achieving high-plex spatial biology, as it does not involve the introduction of additional chemical agents. This approach minimizes the risk of sample damage and helps preserve tissue integrity.

Filtered photobleaching also confers advantages that simplify mIF assay development and increase assay flexibility. The workflow utilizes fluorescently labeled targeting antibodies

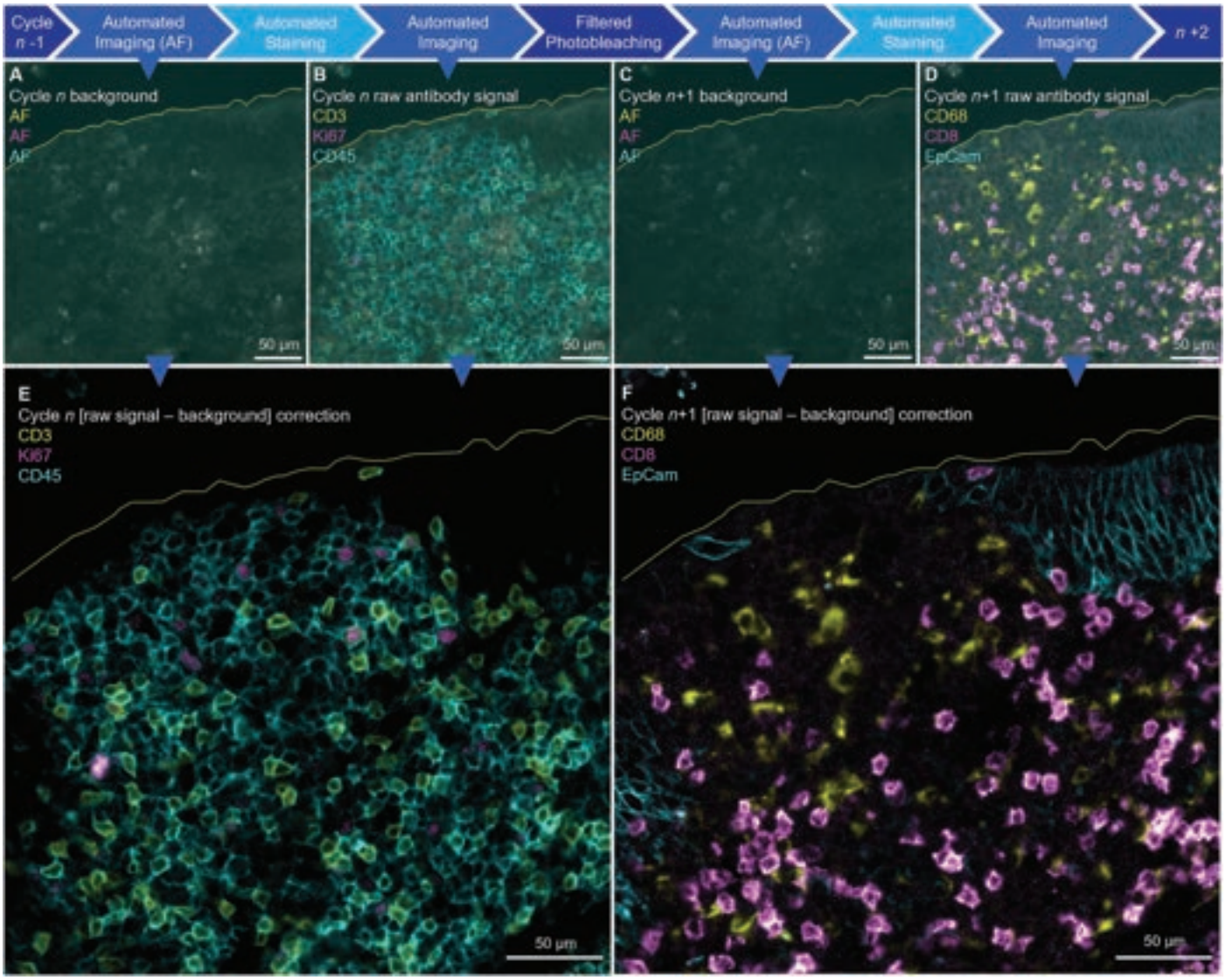

Figure 2: Cyclic mIF data generation with CellScape. All panels show the same location in a human tonsil FFPE section; composite three-channel HDR imaging; yellow line indicates tissue border. A, Composite background autofluorescence (AF) in three channels before cycle *n* auto-staining. B, Automated imaging result after cycle *n* auto-staining. C, Composite background after filtered photobleaching; note the similarity but not exact match to the signal in A, highlighting the necessity for accurate background capture at each cycle. D, $n+1$ cycle auto-staining with new targets. E and F, Results of background (BG) correction of raw images (raw) for cycles *n* and $n+1$, respectively. Note the signal-specific increase in contrast resulting from accurate background subtraction.

directly, without requiring proprietary modifications. This reagent format is ubiquitous, second in availability only to non-conjugated antibodies. When only non-conjugated antibodies are available, established direct-labeling conjugation kits can be used to attach fluorophores; this is particularly useful for niche or novel project-specific targets. Assay design is thus versatile with labeled antibodies being readily available from many vendors.

Using primary antibodies and directly measuring fluorescence also eliminates signal promiscuity, a challenge specific to signal amplification. With direct IF, the fluorescently labeled image can be directly compared to orthogonal gold-standard labeling methods like IHC to supply evidence of matched signal specificity and sensitivity (Figure 5). This is an important standard [7] and can be challenging for oligo-based cycling methodologies. In direct IF, any fluorescence attributed to the fluorophore can be positively assigned to a specific antibody due to the fact that the fluorescing dye is covalently bound to the antibody. Oligo-probe cycling does not confer this benefit. There is high likelihood, but no guarantee, that the hybridization interaction between antibody target and fluorescently labeled oligo-probe has negligible promiscuity among multiple (possibly hundreds) of available oligo targets laid on the sample at once. The same concern is also raised when considering primary-secondary complex removal methods. Secondary detection antibodies cannot discriminate between primary antibodies that were stained during the current cycle of staining and a primary antibody that was inefficiently removed from preceding staining rounds. In these methods there is no *in-process* control to ensure that any residual probe signal is not inaccurately assigned, and it is expected that these concerns would compound with increasing cycle numbers.

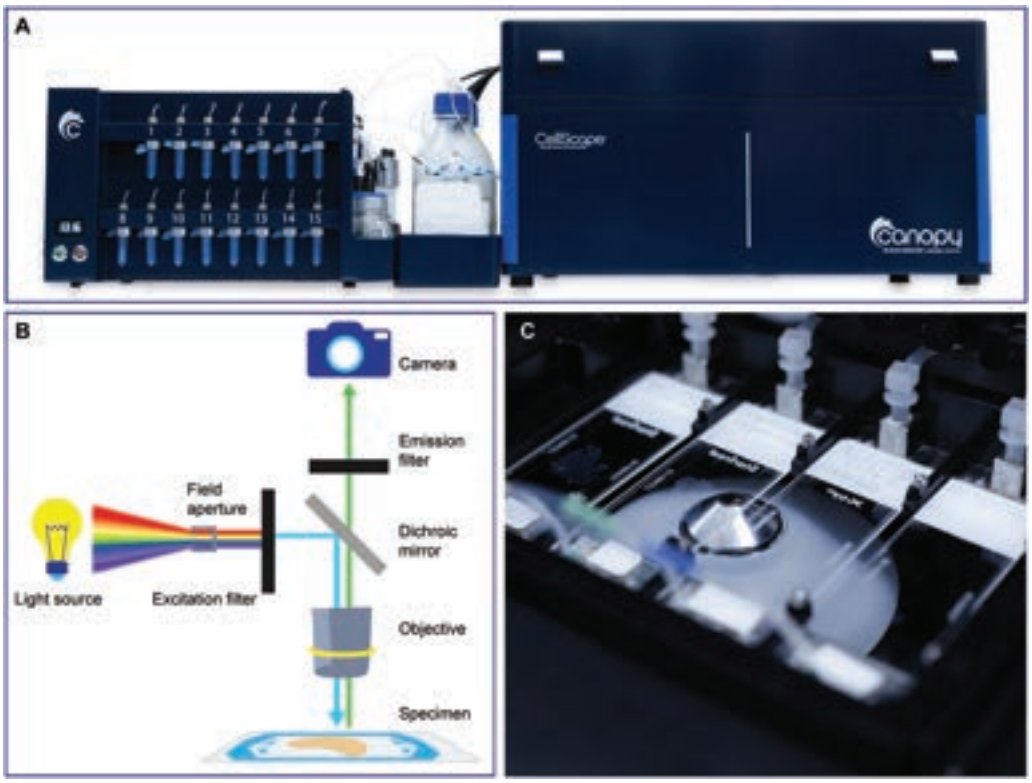

Figure 3: Diagram of CellScape components. A, The CellScape instrument is composed of an integrated fluidics unit, contained automatic microscope, and controlling computer (not shown). The fluidics unit (left), with 15 reservoirs for antibody mixtures, automated immunostaining, and reagent delivery. The microscope box (right), enclosing the optical train (B), and sample carrier (C), automates cyclic mIF data capture, records fluorescence as OME tiff images, and removes fluorescent signals through filtered photobleaching. B, Schematic of light path through the instrument. Briefly, full spectrum excitation light is shaped to precisely illuminate only the camera FOV and passed through an excitation filter/dichroic for wavelength selection. The primary lens is a 20×0.80 NA, 500 μm WD, PlanApo λ D air objective (Nikon Instruments). The same path and excitation source are used for filtered photobleaching. Collected emission is passed through an emission filter and imaged on a CMOS area sensor. Illustration inspired by common depictions of fluorescence microscopy such as Figure 3 in [5] and online resources. C, Close-up of the stage containing the 4-sample holder with CellScape Whole-Slide Imaging Chambers.

Some biologists voice concerns about epitope modification or tissue damage caused by photobleaching, suggesting that light would be an undesirable route to achieve a high-plex dataset. However, the CellScape photobleaching light source is defocused at the sample plane, non-coherent, and filtered to limit the tissue exposure to lower-energy wavelengths (365 nm to 640 nm). Compare this to cyclic complex stripping, where low pH, heat, and pressure are impinged on the tissue repeatedly as an example of physicochemical signal removal, and the argument can be made that filtered photobleaching is an innocuous method of signal removal. In fact, our group (Figure 6) and others [8] have demonstrated tissue integrity after multiple rounds of photobleaching, finding no noticeable degradation via hematoxylin and eosin (H&E) staining.

Finally, multiplexing direct IF via filtered photobleaching obviates any stringent protocol conditions specific to signal removal, increasing the likelihood of successful multi-omic data generation. For example, RNA *in situ* hybridization has been successfully carried out through cyclic filtered photobleaching [9]. Protein-protein interactions, detected via *in situ* proximity ligation assays (isPLA, Navinci Diagnostics), have also been combined with mIF to develop mIF+interaction multi-omic datasets. Figure 7 shows an example of PD1 and PDL1 analyzed with isPLA and imaged on CellScape, positively indicating ligand-receptor interaction.

Microfluidic Imaging Chamber

The heart of the CellScape platform is the CellScape™ Whole-Slide Imaging Chamber (WSIC). The WSIC is a number 1.5-thickness, H-flatness borosilicate glass coverslip mounted on a standard histology slide (25 × 75 mm) (Figure 8). A microfluidic chamber is created by a non-permeable, optically clear, adhesive barrier, which forms a seal around the sample and enables the exchange of fluid for cyclic staining. When mounted on a slide, the WSIC turns any histology slide into a portable microfluidic flow cell. Supporting simplicity and flexibility, the WSIC does not require mounting a specimen onto specialized glass carriers and enables the examination of pre-mounted specimens. Archiving tissue as formalin-fixed paraffin-embedded (FFPE) on histology slides is a widespread practice in biomedical research and clinical pathology. The imaging window, 16 × 44 mm, can accommodate large sections, multi-specimen mounts, and tissue micro arrays.

Flow cells are common in microscopy and critical to many spatial biology methods. They permit the exchange of fluid across a sample for cyclic staining while allowing imaging. Flow cell design must balance competing mechanical and optical requirements. For example, a thicker optical window may make for a more physically robust flow cell, but thicker windows also limit the achievable resolution, where highly resolving optics often have shorter working distances. A common design

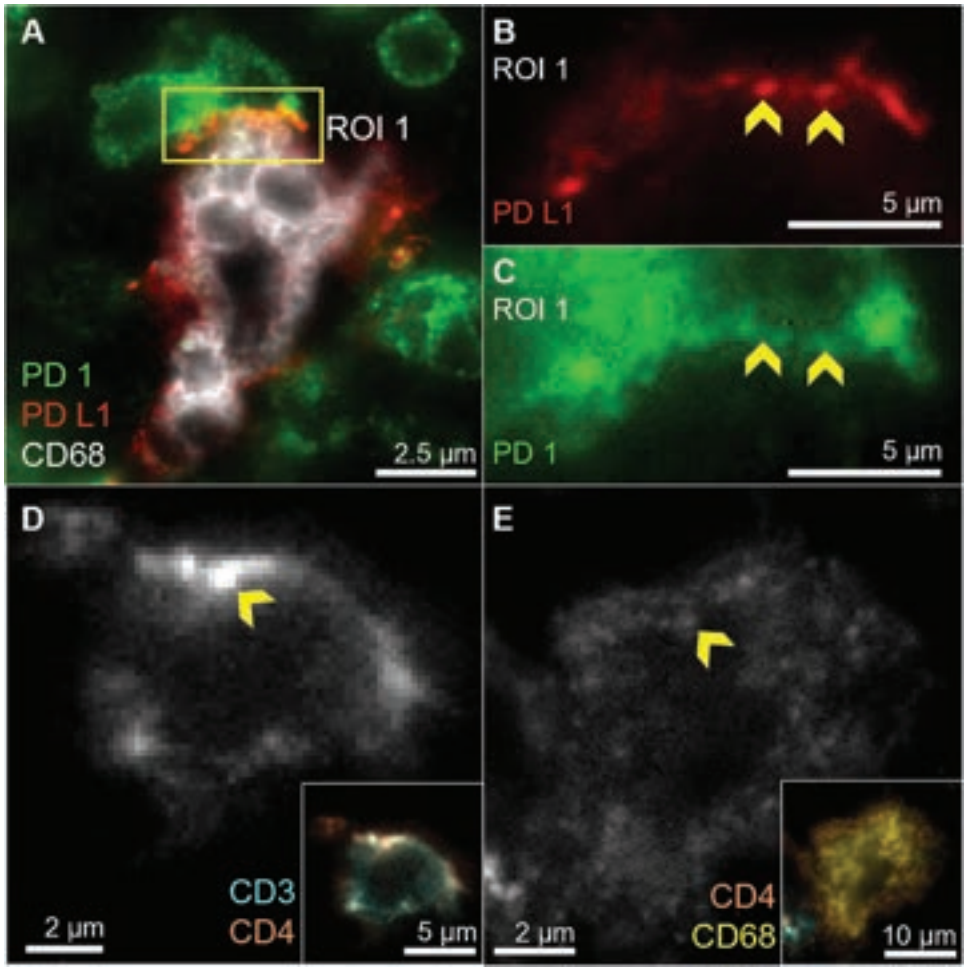

Figure 4: CellScape provides highly resolved, high-contrast images. A–C, Intricate detail in the cell-cell interaction between PDL1 and PD1 expressing cells, including the resolution of discrete PDL1 membrane aggregates (B, arrows). D and E, Two different localizations for a single biomarker, CD4, which is found aggregated to a portion of the plasma membrane (D, arrow) in cells co-expressing CD3 (D, inset, same cell) but diffuse and punctate (E, arrow) in cells co-expressing CD68 (E, inset, same cell).

employs a flow chamber that is integral to the microscope and can be removed from one sample and placed on the next as samples are processed. Conversely, the WSIC is by design self-contained, removable, and storable.

Providing high optical performance while balancing the demands of fluid flow and efficient sample scanning make the WSIC exceptionally valuable in spatial biology, and a remarkable engineering feat. Consider the ideal optical situation of a typical histology preparation, with a short optical path to the sample and a quasi-single refractive index (RI): glass slide, RI-matched mounting media, and coverslip, all in direct contact. Instead, flow introduces a water column between the sample and coverslip, inducing RI aberration. The optical system of the CellScape maintains the performance of a 0.80 NA air objective even when imaging through 50+ µm of buffer, as evidenced in Figures 1 and 4 above.

Versatile, Modular Reagents

Assays must remain flexible, but for those new to spatial biology validated assays are equally important. Reagent kits and paired assays fill this need. VistaPlex™ assay kits include antibodies that are commercially available, widely applicable, and supported by an extensive validation process. Rigorous validation includes confirmation of broad tissue suitability (Figure 9A), qualitative assurance that biomarker specificity matches expected target inclusion and exclusion (Figure 9B), and quantitative evidence of reproducibility across labs performing the assay (inter-assay) as well as replication of the assay over time (inter-assay) (Figure 9C). Additionally, by grouping biomarkers into kits to answer specific questions, for example, "What is the immune composition of the tumor?" or "What is the metabolic state of the tumor?", this ecosystem of kits aligns with hypothesis-driven re-examination (see *Data-Driven Assay Expansion* section). This characteristic, extensive validation, and easy incorporation of project-specific probes, together provide a powerful tool for translating hypotheses into pragmatic assays.

Data-Driven Assay Expansion

The CellScape enables a flexible, data-driven approach to high-plex spatial biology. The WSIC is designed for safe storage of a sample. When combined with filtered photobleaching and direct IF labeling, it allows multiple rounds of iterative analysis, punctuated by periods of storage. This is unique, and in contrast to other mIF techniques, where cycling methods either do not

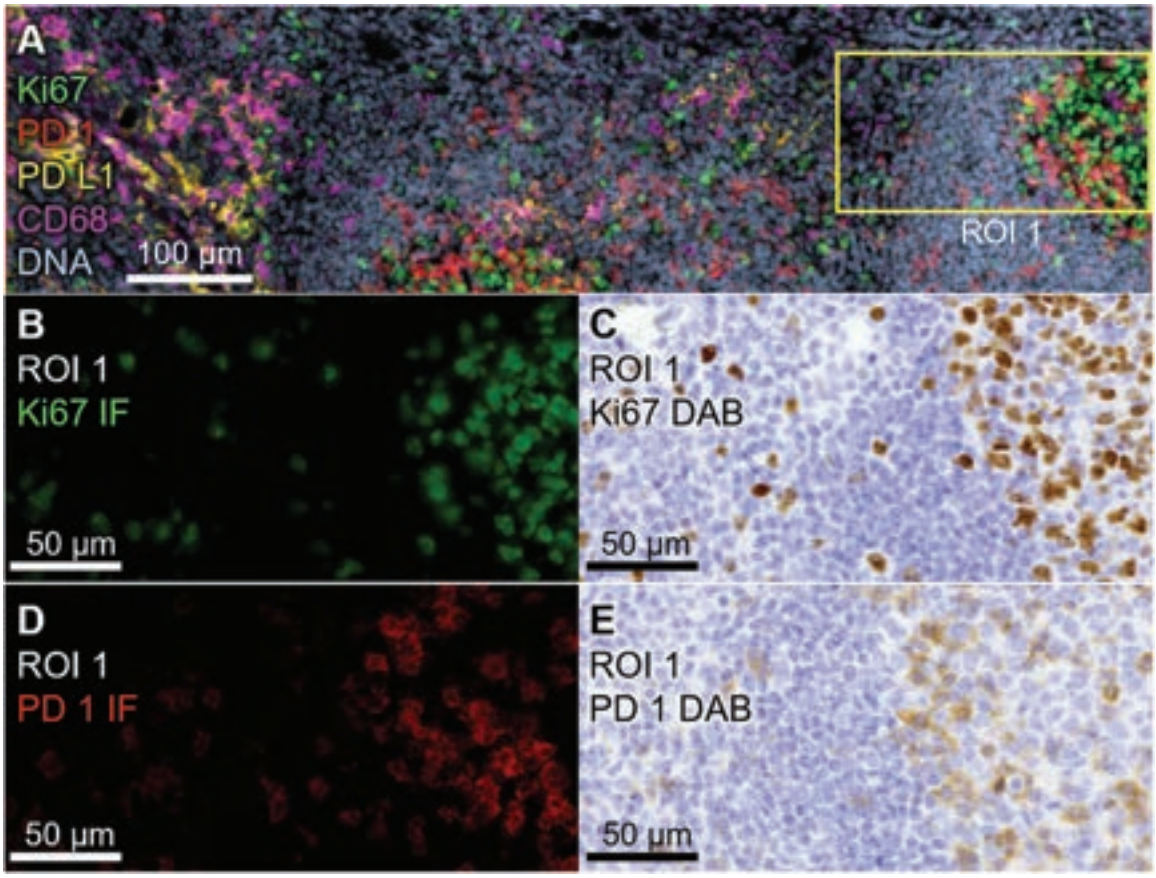

Figure 5: Correlation of mIF antibody performance. Direct comparison of CellScape mIF data using primary-conjugated antibodies to DAB colorimetric data collected from adjacent serial sections of the same human tonsil FFPE biopsy (unconjugated antibodies). A, mIF composite of five biomarkers. ROI 1 highlighting a single tonsillar germinal center. B, ROI 1 from A, showing one of five channels in A corresponding spatially to C; DAB staining for the same biomarker in an adjacent serial section. Brown coloration indicates positive staining. Spatial correspondence between B and C allow for direct comparison and validation of signal specificity and sensitivity in mIF. D and E are like B and C but depict a different biomarker.

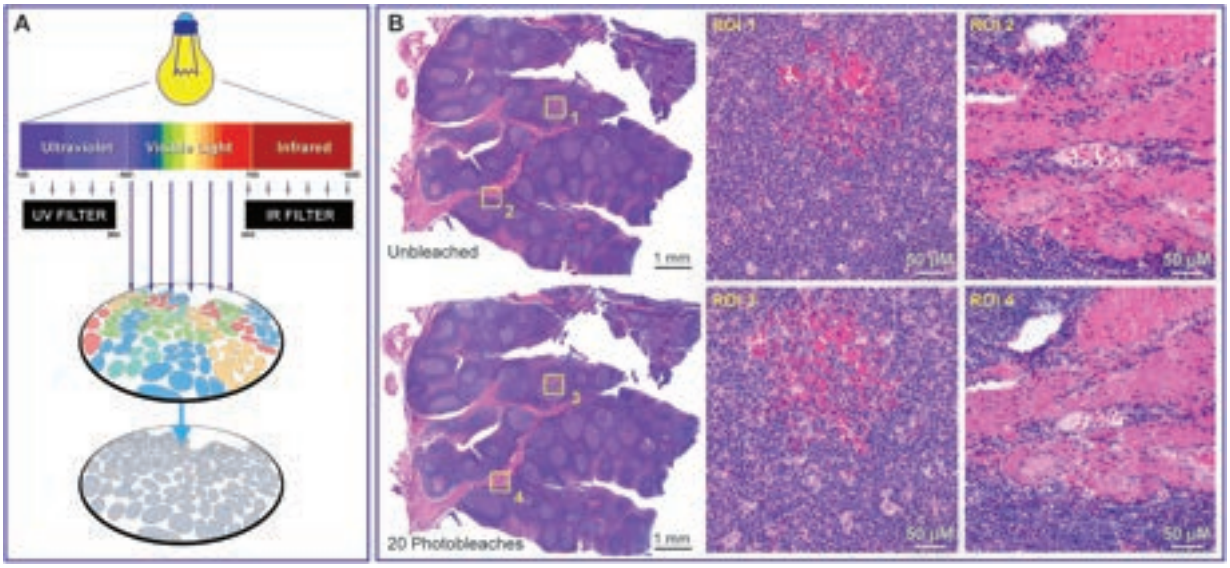

Figure 6: Filtered photobleaching. A, Schematic for filtered photobleaching, which only passes visible wavelengths to protect tissues from UV damage. B (top and bottom), Adjacent serial sections of human tonsil FFPE tissue. B (top row), Section without any photobleaching. B (bottom row), Serial section after twenty 20-second rounds of photobleaching (400 seconds total). ROIs in B show comparable staining and morphology seen before and after filtered photobleaching at whole-tissue and single-cell scales.

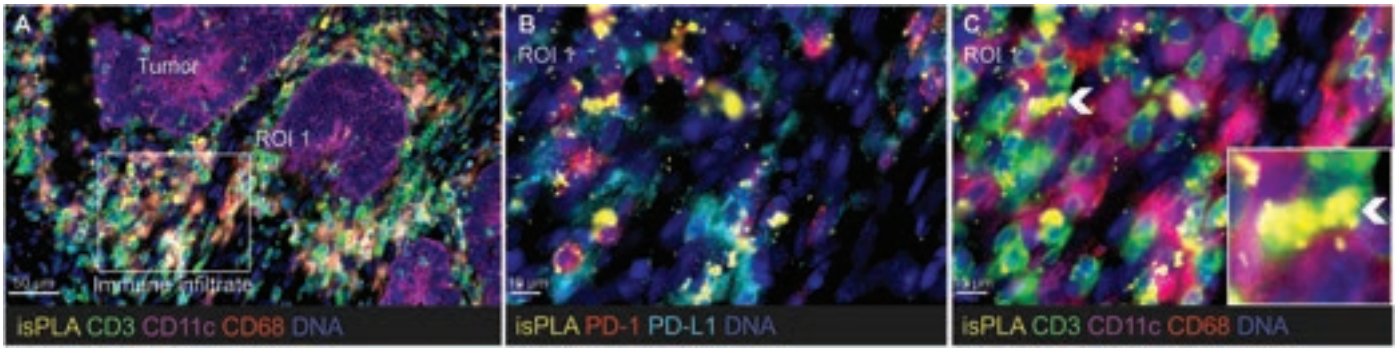

Figure 7: mIF is augmented by adding interactome data gathered through isPLA. Combined isPLA and mIF staining in a human colorectal carcinoma FFPE tissue. The Naveni PD1/PD-L1 isPLA kit (Navinci Diagnostics, Uppsala, Sweden) was used to visualize protein-protein interactions between PD-1 and PD-L1 alongside an 18-plex mIF assay to identify cell populations. A, Overview of the tumor sample and a surrounding immune infiltrate. While PD-L1 staining was not present on tumor cells (not shown), PD-1 and PD-L1 staining is present in immune infiltrate areas in the stroma around the tumor regions as shown in B. These immune infiltrates are also enriched in isPLA signal (yellow), suggesting PD-1/PD-L1 interaction and checkpoint activation. High-magnification images in B and C also show that PD-L1 staining co-localizes with CD68 and CD11c, while PD-1 staining co-localizes with CD3 signal. The isPLA signal is localized to the interface between CD3+ and CD68+ immune cells (arrow and inset), suggesting a tumor-associated macrophage mediated immunosuppression.

easily permit additional primary antibody staining or do not support high cycle number due to sample degradation. Pausing between cycles affords the researcher the ability to examine the data, form additional hypotheses, then retrieve the same sample from storage to apply more probes aimed at exploring those hypotheses. This may be repeated over days, weeks, or months following the initial staining rounds. With the WSIC, it is thus possible to gather data on the quality of a tissue before wasting resources on sections with excessive necrotic or acellular regions. Storage of samples after analysis also ensures that

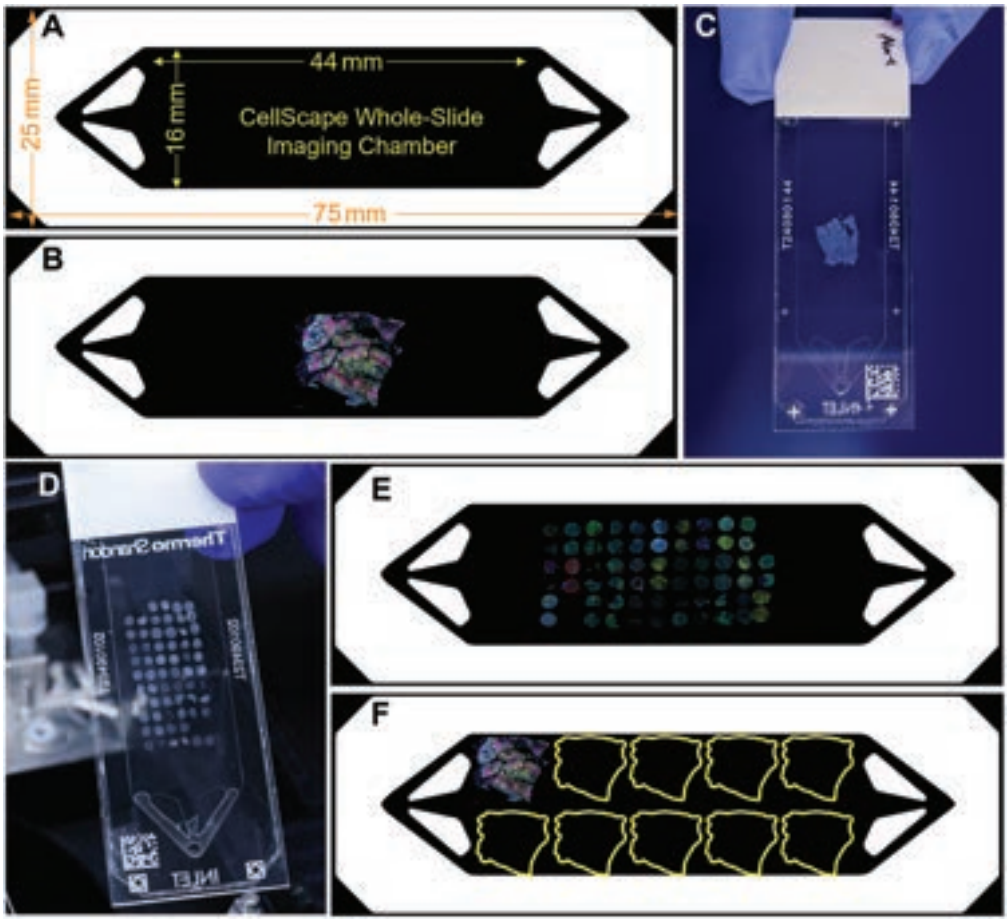

Figure 8: CellScape Whole-Slide Imaging Chamber (WSIC) capabilities. A, Graphic of WSIC with dimensions of imaging area as shown. Flow diverters ensure a uniform delivery of reagents across the image chamber. The versatile WSIC can be used for large tissue sections (B, C) or tumor microarray samples (D, E). Additionally, serial section replicates (shown as yellow traces) can be placed on the same slide to reduce batch effects (F).

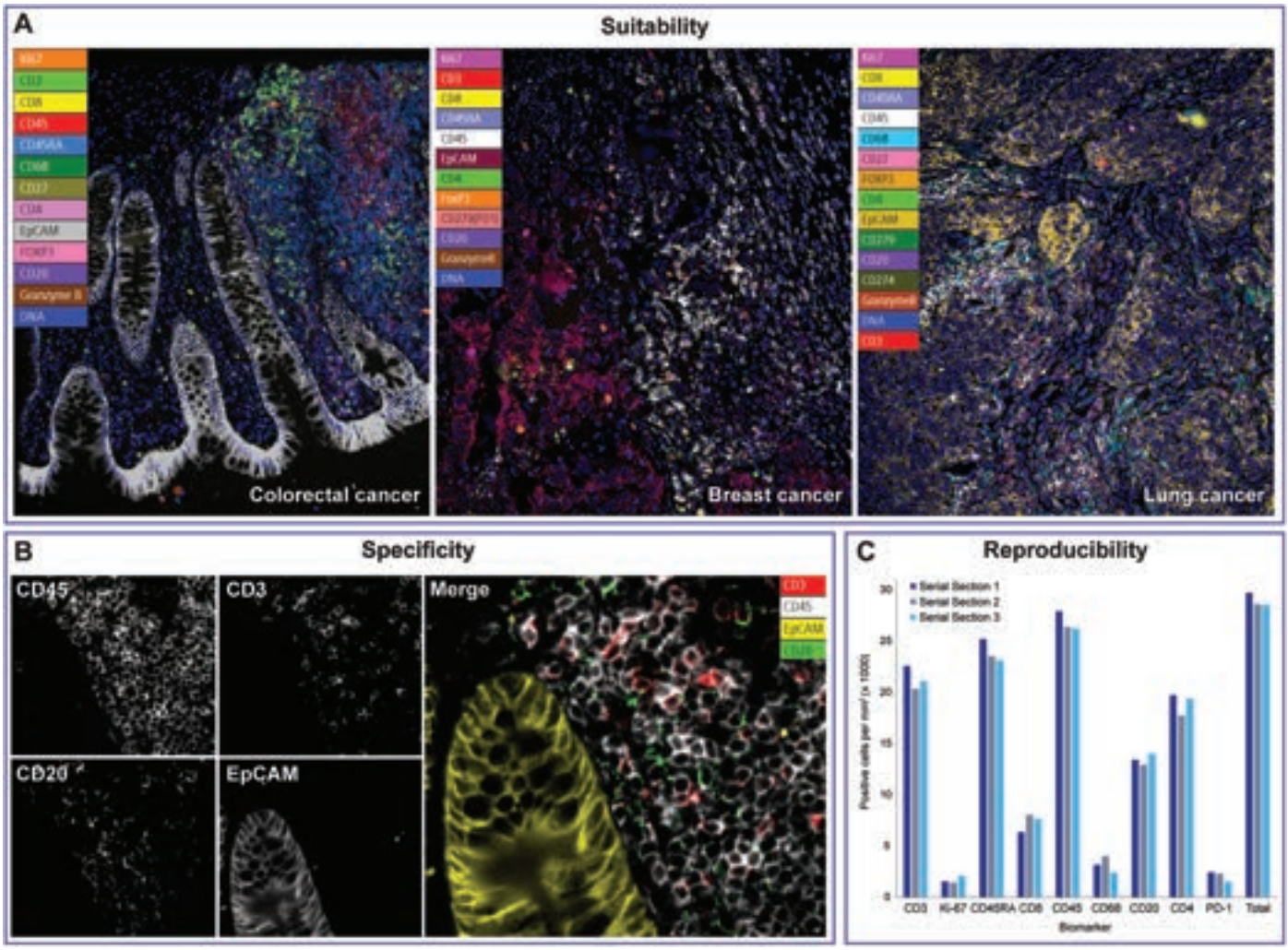

Figure 9: Antibody panel validation is a rigorous process. A, High-contrast multi-channel composite images of multiple tissue types demonstrate broad suitability and/or applicability of panel detection reagents across human FFPE tissues. B, Four panels depict signal compartmentalization to expected target cell populations. Note that CD45 defines all smaller immune cells while avoiding larger columnar cells seen in EpCAM, while CD3 and CD20 define other subsets of immune cells. The merged image highlights the expected overlap and exclusion of signal based on *a priori* knowledge of antibody specificity and confirms staining specificity. Note the overlap of CD45, expressed in most lymphocytes, with both CD3+T cells, and CD20+ B cells, and the mutual exclusion of CD3 and CD20 signal. C, The number of positive cells per mm² derived from image segmentation, single-cell biomarker measurement, and threshold gating demonstrates reproducibility of the assay. Serial sections taken from a single FFPE tonsil tissue and processed by three different operators with three different CellScape units. Low variability among replicates demonstrates high reproducibility.

precious or rare samples are not wasted by using non-optimal assay panels or destructive analysis methods. The data always guide the assay.

To illustrate the value of data-driven assay expansion, we examined a resection biopsy from a patient diagnosed with a lung adenocarcinoma. Our first staining experiment included general tissue profiling with fourteen antibodies comprising the VistaPlex™ Spatial Immune Profiling Kit, designed to identify major immune cell classes and demarcate epithelial tissue. We then stored the sample at 4°C and examined the resultant data (Figure 10A). Upon initial inspection, regions of strong immune infiltration can be identified as organized aggregates of immune cells enriched for CD68 and CD20 (Figures 10B–E), indicating the presence of organized immune cell clusters known as tertiary lymphoid structures (TLS). Additional staining of *the same slide* was conducted for dendritic cell lineage, vasculature, and stroma, and upon further inspection, the presence of mature TLS was confirmed. The presence of dendritic cell markers in these aggregates affirms germinal center-like character (Figure 10F), a defining feature of TLS. Vascularization is another strong indicator of TLS presence (Figure 10G). In total, thirty-four markers were deployed on this tissue over a month-long period through iterative and hypothesis-driven staining followed by data examination, and the sample is still available for additional examination at the time of this writing.

Forming Precise Images

The CellScape instrument with its whole-slide capability is specifically designed for precise image capture and quantitative phenotyping of large sample areas such as tissue microarrays and intact whole biopsies. Precision over such scale is achieved through incorporation of highly acute optics, high pixel density detection, and multi-exposure high-dynamic-range (HDR) image capture.

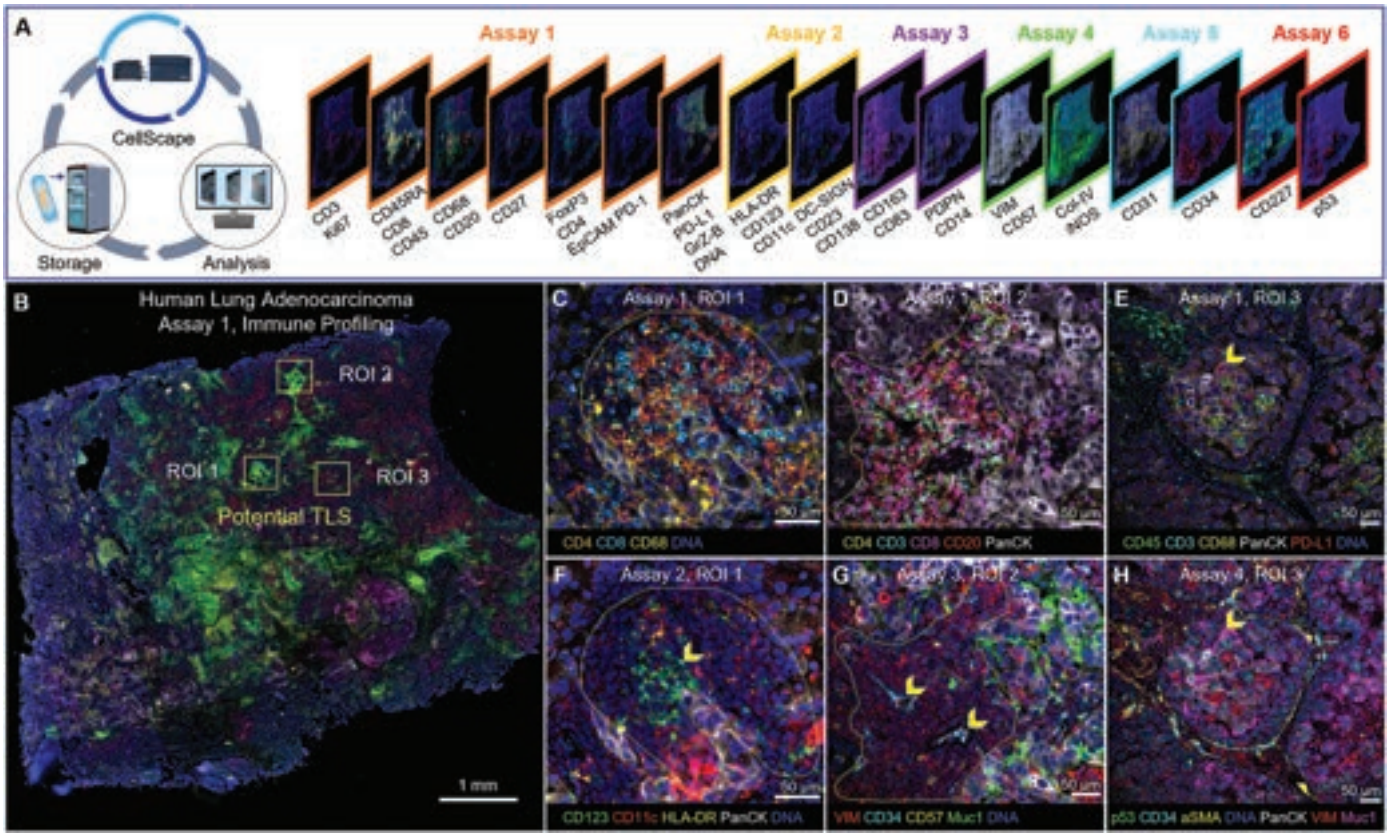

Figure 10: Data-driven assay expansion. A single human lung adenocarcinoma FFPE section interrogated for thirty-four markers over a period of weeks, built through data-driven assay development and deployment. A (left), Cyclic workflow of analysis and storage, with each subsequent assay occurring after a period of sample storage; border color indicates reinterrogation assay number. B, Whole section sampling and location of ROI 1, 2, and 3 containing suspected TLS inclusion based on results of Assay 1: VistaPlex Spatial Immune Profiling panel. C and D show detail of ROI 1 and 2 highlighting large aggregations of CD4 and CD8 cells intermingled with CD68 and CD20 indicative of putative TLS (yellow dotted margin). E, ROI 3, in contrast, does not indicate TLS for lack of these features, (yellow arrow PD-L1 positive cell). F, Presence of CD123 (yellow arrow), CD11c, and HLA-DR affirm dendritic cell presence, a TLS hallmark. G, Presence of CD34 (yellow arrows) indicates vascularization of the structure, a sign of TLS maturity. H, Additional reinterrogation data examining disease drivers, highlighting the close association of p53, Muc1 (yellow arrow), and PD-L1.

Before digital sampling, higher NA optics form sharper images and more efficiently collect signal, resulting in higher sensitivity to dim signals and less time required for signal integration. Sharpness is commonly described by the Rayleigh resolution criterion: $0.61 * \lambda/NA$. Collection of emission down to ~400 nm through a 0.80 NA lens puts a rough limit on feature resolution at: $0.61 * 400\ nm/0.80\ NA = 0.300\ \mu m$. High NA light collection also improves image contrast and collection efficiency. Here brightness is the typical measurement: $NA^4/Magnification^2 = Brightness$. Combinations of low magnification and high NA are most efficient. For example, while a 40×0.95 NA objective provides a modest 15% increase in resolution over a 20×0.80 NA objective, the 20×0.80 NA will be 200% more sensitive at the same exposure length, or conversely, it will capture the same intensity at 50% of the exposure length, speeding up image collection. The 20× objective will also scan the same sample area in 1/4th the time relative to the 40×: $(AREA/20)^2/(AREA/40)^2 = 0.25$ (Table 1 and Figure 11). CellScape thus forms a highly resolved, high-contrast image as a necessary substrate for digital capture and quantification.

In digital microscopy, measurement precision is limited by the spatial sampling frequency of the detector. Our bright, sharp image formed through high NA and low magnification presents a challenge to digital area scan detectors, explained by the Nyquist criterion: Optimal sampling = feature length/2.3. Resolving a 0.300 µm feature requires a sampling period of 0.300 µm/2.3 = 0.130 µm, which at 20× requires a tiny camera pixel: 20× * 0.130 µm = 2.6 µm. Sensors with such a small

Table 1: Optical parameter comparisons for objectives common in spatial biology.

Mag	NA	Resolution/Nyquist/Req. Pixel [nm/nm/µm]			Relative Brightness	FOV (mm²)	Relative Time to Scan
		λ 400 nm	λ 550 nm	λ 750 nm			
20	0.70	349/152/3.03	479/208/4.17	654/284/5.68	0.59	0.813	1.7
20	0.80	305/133/2.65	419/182/3.65	572/249/4.97	1.00	0.813	1.0
40	0.95	257/112/4.47	353/154/6.14	482/209/8.38	0.50	0.203	8.0

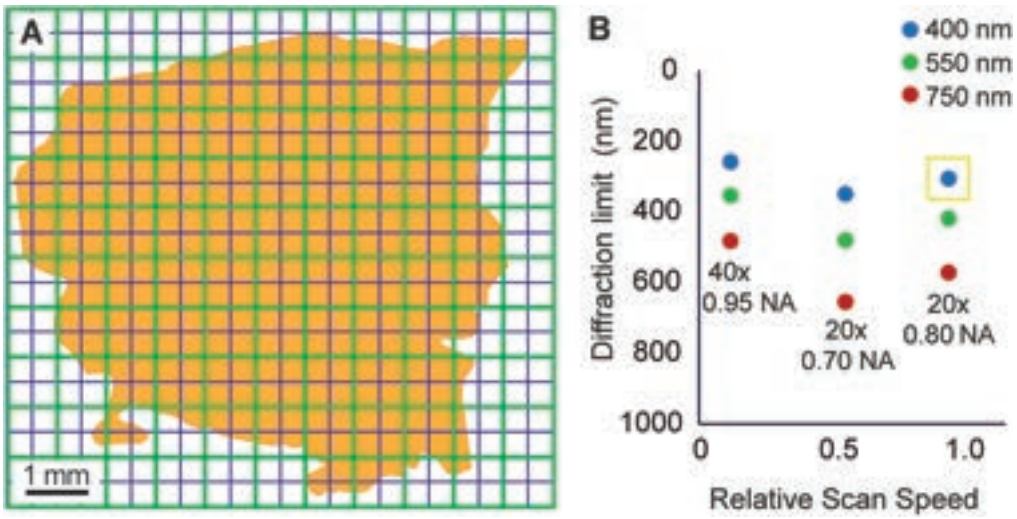

Figure 11: Comparison of performance of common objectives. A, Representation of a tissue section scanned by a 40× (blue grid) and a 20× (green grid) objective, illustrating the 4:1 FOV ratio between the two objectives. B, Comparison of diffraction limit versus relative scan speed for the objectives in Table 1 at three different wavelengths (blue/green/red dots). Yellow box indicates optimal performance of 20×, 0.80 NA objective, maintaining 85% the resolution of a 40× objective while scanning 8× faster.

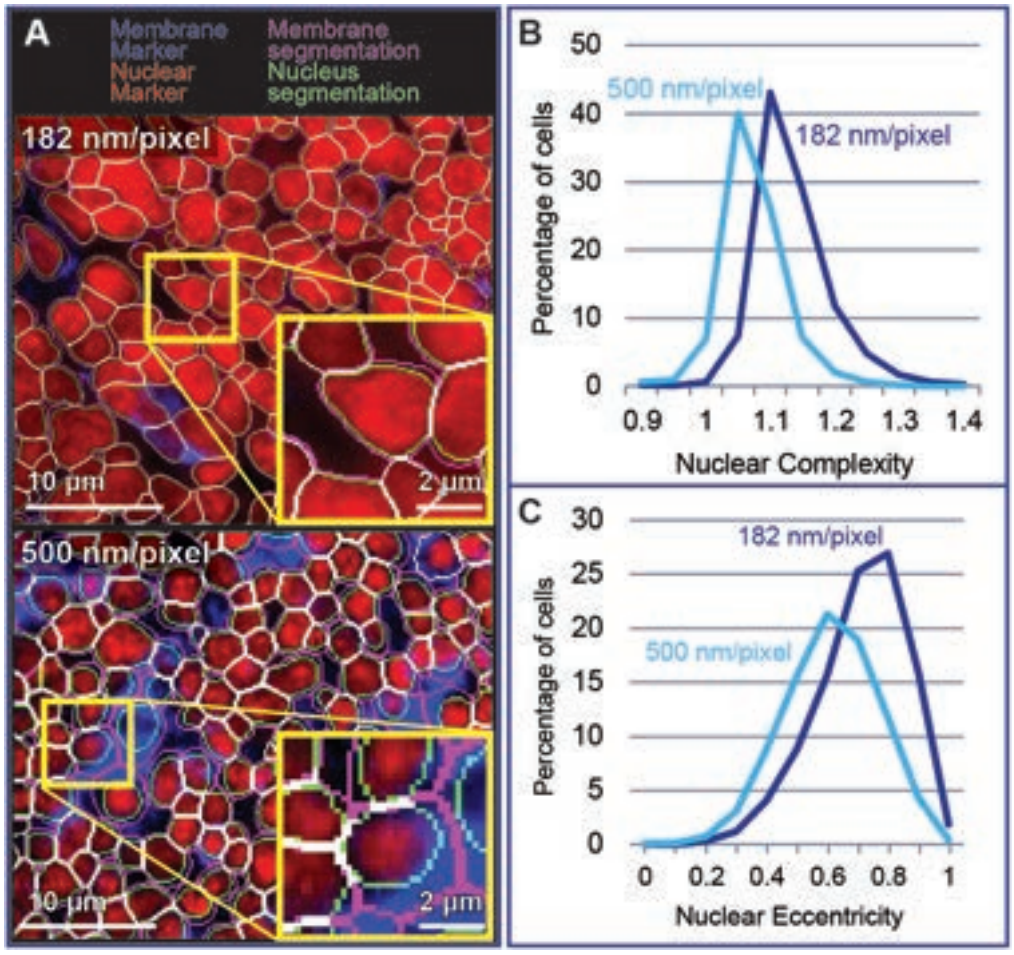

Figure 12: Higher digital sampling enables greater fidelity in image analysis. A, Data collected from two tonsil samples matched in assay parameters and in primary objective mag/NA but differing in digital sampling rate. A (top), 182 nm/pixel; (bottom), 500 nm/pixel. Both datasets were segmented with Mesmer [10]. B, Digital sampling rate versus nuclear shape complexity: nucleus perimeter/perimeter of circle having matched nucleus area. C, Digital sampling rate versus nuclear shape eccentricity: distance of nucleus centroid from cell membrane centroid. Both nuclear parameters are increased with 182 nm/pixel digital sampling, indicating a conferred benefit to segmentation fidelity.

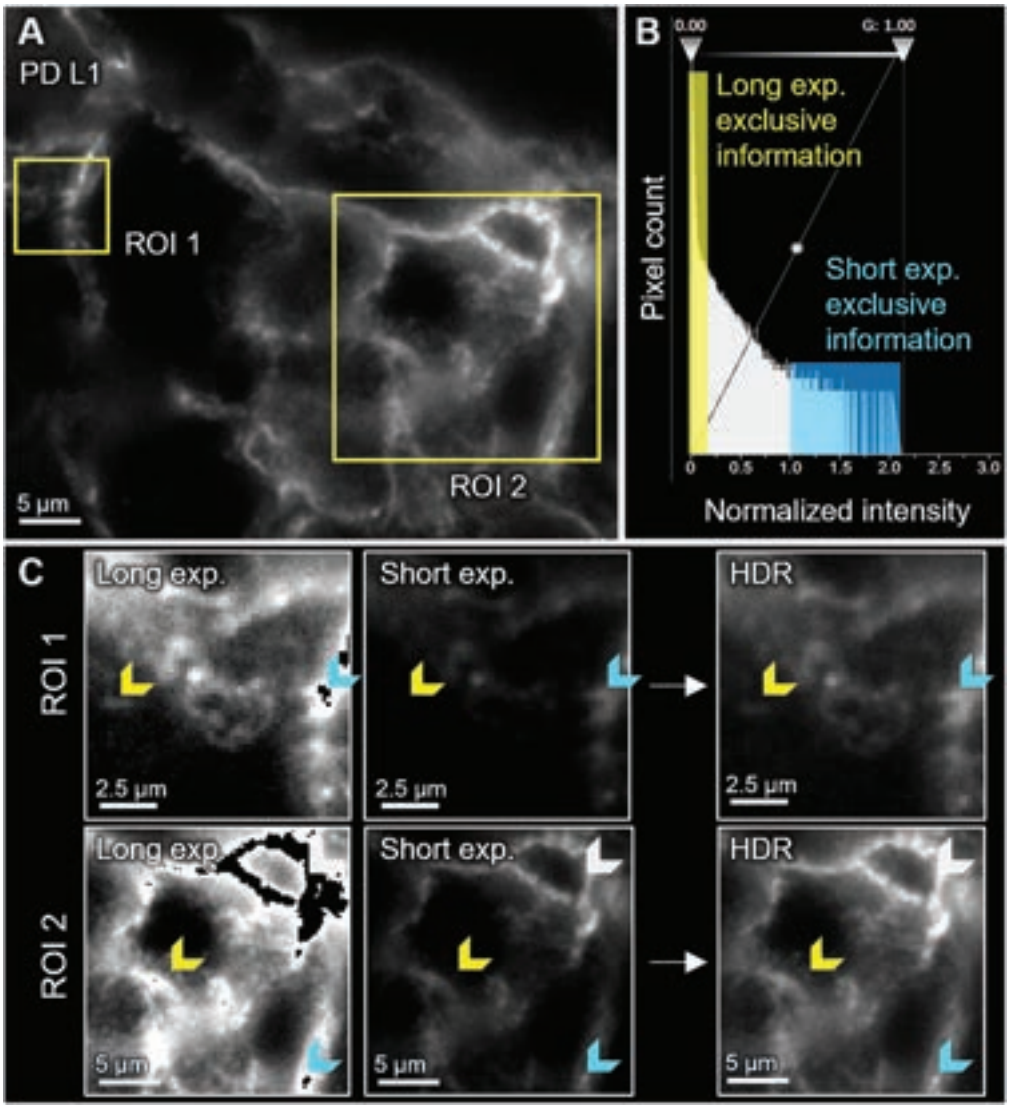

Figure 13: HDR imaging improves image contrast in mIF spatial biology data. All panels, PDL1 staining human hyperplastic tonsil. A, HDR composite highlighting retained detail over all captured intensities (yellow ROI 1 and 2, and C, right). B, Histogram of intensities from A normalized to longest exposure in the series illustrates intensity values contributed exclusively by short (blue highlight) and long (yellow highlight) exposures in HDR composite. C, ROI 1 and 2 from A (left), long exposure captures dim fine structure (yellow arrows) but omits bright signal (blue arrows). Middle, shorter exposures miss dim fine structure but capture bright signal.

pixel size and a sensor array large enough to fully capitalize on the FOV of a 20× objective have only been available in the last few years. The effective pixel pitch of 0.182 µm satisfies the criteria at emission wavelengths $\geq$ 525 nm, while maintaining a sampling area of > 0.813 mm^2, providing a high-fidelity image while meeting the throughput requirements of spatial biology. Pixel-sampling dictates the granularity of expression and localization data encoded in the digital image, limiting analysis precision.

Cell segmentation, the division of a whole tissue image into individual, distinct cells for single-cell analysis, is a key challenge that must be addressed by spatial biology technologies. The clarity of images obtained on CellScape enables more accurate segmentation than using a system with lower-resolution image capture. We compare the data collected from two systems, both collecting through a 0.80 NA 20× objective, but digitally sampled at either 0.500 µm/pixel or 0.182 µm/pixel (Figure 12). Using the same segmentation algorithm for both image sets, we demonstrate a marked increase in nuclear complexity coming from finer digital sampling. The increase found equates to higher image segmentation fidelity, a fundamental and practical benefit for increased digital sampling. Most tissue image segmentation techniques use nuclear shape as a kernel. Achieving high pixel density in a high-NA, low-magnification system allows for efficient sampling and a more granular division of objects, avoiding imprecision through under-sampling.

Quantitative Data Collection

Due to controlled assay parameters and purposeful signal amplification, spatial biology is generally not a light-limited application. Long exposures enhance sensitivity for capturing

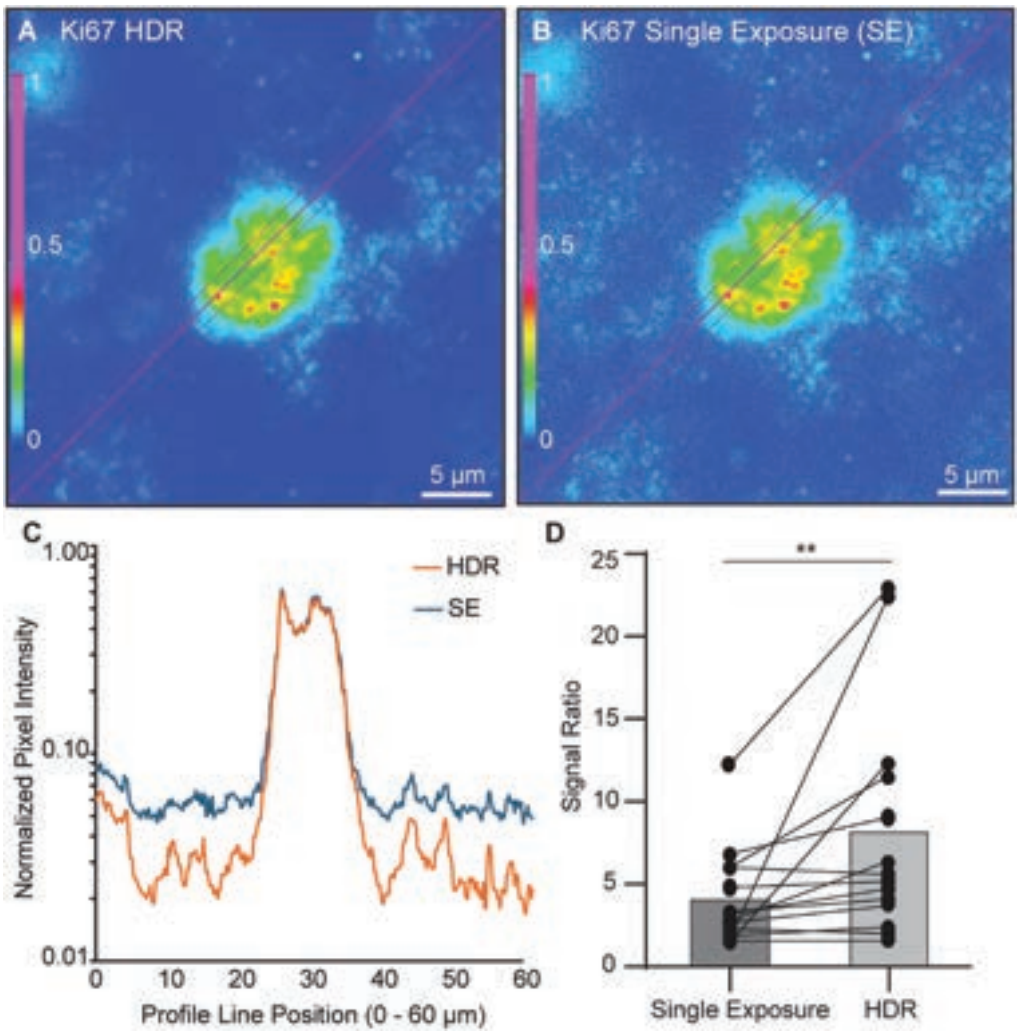

Figure 14: HDR imaging improves SNR in background subtraction. A and B, Ki67 signal after pixel-wise linear subtraction of an unstained background image. Both depict the same scene, where A integrates all information in an HDR series, and B only includes the longest exposure possible while avoiding saturated pixels. Both images are normalized to the maximum intensity in the image. Pseudo-coloring indicates normalized intensity with indicated mapping (panel bottom). Pink line indicates the position of intensity profile in panel C, 0 µm (lower left corner), 60 µm (upper right corner). C, Intensity across the profile line in A and B (pink line). Overlapping intensity information in HDR and SE across the bright Ki67 cell (center ~25 to 35 µm) comes from the same shorter exposure. Divergence in lower intensities results from HDR data series incorporating values from longer exposures below the noise floor of the SE. D depicts this effect over multiple biomarkers on a signal tissue. Signal ratio compares average intensity between cells positive for a marker and cells negative for that marker. Connected dots represent corresponding biomarkers.

fine details, but they also risk introducing over-exposed pixels (Figure 13). Multi-exposure HDR imaging is a method for capitalizing on the sensitivity of the system while solving the problem of over-exposure. The utility of any scientific camera is limited to signal within its linear response range. Signal below (noise) and above (oversaturation) this range is not quantifiable. Conversely, within the linear range, the response is consistent: detected intensity = true scene luminescence * camera-response-function (CRF). The CRF, primarily determined empirically, is generally linear with respect to exposure time. Doubling the exposure time will double the recorded intensity. And conversely, halving the exposure length (for example, to bring signal into the linear response range of the camera) will halve the recorded intensity. This provides a way to integrate signal across exposures and capture biological expression that requires multiple different exposure lengths to record [11].

A useful consequence of HDR imaging in spatial biology is the preservation of detail after auto-fluorescence subtraction. Tissue contains various highly fluorescent materials, including collagen, red blood cells, lipofuscin, and melanin. Autofluorescence is further exacerbated by FFPE preparation, and the digital subtraction of background fluorescence is therefore commonplace. In a single-exposure capture system, high background signals necessitate shorter exposures to prevent over-saturation. However, shorter exposures reduce system sensitivity, resulting in missed fine details and muted fluorescence differences. HDR imaging, with its expanded dynamic range, allows for improved signal preservation after background signal subtraction and ultimately more accurate detection of true biomarker signals (Figure 14).

HDR confers multiple practical benefits to spatial biology research including better signal detection after

background subtraction, increased image contrast, and finer intensity discrimination in cases where signal quantification is required to delineate phenotypes, such as CD4 and PDL1 in the examples above. Finally, because the exposure parameters are constant, we eliminate tedious exposure optimization, a requirement for other spatial biology platforms. This benefits efforts to normalize over large sample cohorts. Wider expression capture also affords greater tolerance to biological variation.

High-precision optics and high-density sampling, in combination with HDR imaging, achieve a design that is precise and quantitative without unacceptable compromise in sample throughput.

Conclusion

The CellScape Precise Spatial Multiplexing platform represents a significant and powerful re-imagination of spatial biology data collection that is centered around exploring targeted research questions. High-plex biomarker expression and localization datasets are built with data-driven feedback. Validated and flexible reagent kits support this approach, allowing program-specific probe inclusion while also providing a consistent background of canonical markers suitable for cross-sample, and even cross-tissue, comparison. Finally, high resolution, HDR image capture from TMAs, large biopsies, and pre-slided clinical samples, ensure the complete and accurate reproduction of morphology and expression patterns. Thus, the CellScape platform, an integrated microscope and in-process stainer, is an elegant and powerful tool for generating spatial biology data.

Acknowledgment

JSS, DJS, MHI, STL, KC, CJ, AC, JAS, BB, TDC, and OB are employed by Bruker Corporation.

References

[1] N de Souza et al., *Nat Rev Cancer* 24 (2024) https://doi.org/10.1038/s41568-023-00657-4.
[2] D Bressan et al., *Science* 381 (2023) https://doi.org/10.1126/science.abq4964.
[3] CR Stoltzfus et al., *Cell Rep* 31 (2020) https://doi.org/10.1016/j.celrep.2020.107523.
[4] C Hennig et al., *Cytometry* 75A (2009) https://doi.org/10.1002/cyto.a.20668.
[5] JW Lichtman and JA Conchello, *Nat Methods* 2 (2005) https://doi.org/10.1038/nmeth817.
[6] D Schapiro et al., *Nat Methods* 19 (2022) https://doi.org/10.1038/s41592-021-01308-y.
[7] S Jarosch et al., *Cell Rep Methods* 1 (2021) https://doi.org/10.1016/j.crmeth.2021.100104.
[8] JR Lin et al., *Nat Cancer* 4 (2023) https://doi.org/10.1038/s43018-023-00576-1.
[9] S Jarosch et al., *STAR Prot* 3 (2022) https://doi.org/10.1016/j.xpro.2022.101374.
[10] NF Greenwald et al., *Nat Biotechnol* 40 (2022) https://doi.org/10.1038/s41587-021-01094-0.
[11] C Vinegoni et al., *IEEE J Sel Topics Quant Elect* 25 (2018) https://doi.org/10.1109/JSTQE.2018.2881608.

MT